Plasma parameter scaling of the error-field penetration threshold in tokamaks

Richard Fitzpatrick

Citation: Physics of Plasmas (1994-present) **10**, 1782 (2003); doi: 10.1063/1.1560924
View online: http://dx.doi.org/10.1063/1.1560924
View Table of Contents: http://scitation.aip.org/content/aip/journal/pop/10/5?ver=pdfcov
Published by the AIP Publishing

Plasma parameter scaling of the error-field penetration threshold in tokamaks[a)]

Richard Fitzpatrick[b)]
Center for Magnetic Reconnection Studies, Institute for Fusion Studies, Department of Physics, University of Texas at Austin, Austin, Texas 78712

(Received 31 July 2002; accepted 23 January 2003)

A previously published analytical formula for the error-field penetration threshold in rotating tokamak plasmas is successfully benchmarked against nonlinear magnetohydrodynamical simulations in slab geometry. Moreover, the fundamental assumption underlying the derivation of this formula, namely, that the response of a flowing plasma to a low amplitude, quasistatic, resonant magnetic perturbation is governed by *linear*, *constant-ψ* layer physics, is verified over a wide range of plasma parameters, which includes the parameter range relevant to Ohmic and neutral beam injection start-up discharges in modern-day tokamaks. It is concluded that the formula in question can be used to estimate error-field penetration thresholds in such plasmas. © *2003 American Institute of Physics.* [DOI: 10.1063/1.1560924]

I. INTRODUCTION

Tokamak plasmas are invariably subject to small amplitude, static, resonant magnetic perturbations—known as ''error-fields''—which are generated primarily by field-coil misalignments and nonaxisymmetric coil-feeds. Such perturbations can significantly degrade energy confinement by driving magnetic reconnection (and, hence, magnetic islands) in intrinsically tearing-stable plasmas. Error-field driven reconnection is strongly suppressed by the naturally occurring toroidal rotation in tokamak plasmas. However, when the error-field amplitude rises above a certain critical value, the plasma rotation is suddenly arrested, and error-field driven reconnection proceeds unhindered—this effect is known as error-field ''penetration.'' The scenario outlined above has been observed experimentally in a number of tokamaks.[1–3]

An analytic theory has been developed which predicts the critical error-field amplitude above which driven reconnection is triggered in a rotating, tearing-stable tokamak plasma.[4–6] One disturbing aspect of this theory is that the critical amplitude decreases rapidly with increasing machine size, suggesting that next-step tokamaks may be hypersensitive to error-fields. Since practical error-field alleviation mechanisms in next-step devices are all extremely costly, it is important that this theoretical scaling be tested as thoroughly as possible.

This paper describes a number of nonlinear, two-dimensional, slab, resistive, viscous, magnetohydrodynamical (MHD) simulations designed to investigate the scaling of the critical error-field amplitude with plasma parameters. Section II outlines the basic system of equations used in these simulations. The application of the aforementioned analytic theory to the investigation is described in Sec. III. The numerical simulations themselves are presented in Sec. IV. Finally, the paper is summarized and conclusions are drawn in Sec. V.

II. PRELIMINARY ANALYSIS

A. Basic equations

Standard right-handed Cartesian coordinates (x,y,z) are adopted. It is assumed that there is no variation along the z-axis, i.e., $\partial/\partial z \equiv 0$. Consider a compressible plasma governed by equations of resistive, viscous, MHD. Let the plasma density, ρ, and viscosity, μ, both be uniform, and let the resistivity, η, be a function of x only. It follows that

$$\mathbf{B} = \nabla \wedge \mathbf{A}, \tag{1}$$

$$\mu_0 \mathbf{J} = \nabla \wedge \mathbf{B}, \tag{2}$$

$$-\frac{\partial \mathbf{A}}{\partial t} - \nabla \varphi + \mathbf{V} \wedge \mathbf{B} = \eta \mathbf{J} - \mathbf{E}_0, \tag{3}$$

$$\rho\left[\frac{\partial \mathbf{V}}{\partial t} + (\mathbf{V}\cdot\nabla)\mathbf{V}\right] = -\nabla p + \mathbf{J} \wedge \mathbf{B} + \mu \nabla^2 \mathbf{V} + \mathbf{F}_0, \tag{4}$$

$$\frac{\partial p}{\partial t} + \mathbf{V}\cdot\nabla p = -\Gamma p \nabla \cdot \mathbf{V}, \tag{5}$$

where $\mathbf{A}$ is the vector potential, φ is the scalar potential, $\mathbf{B}$ is the magnetic field, $\mathbf{V}$ is the plasma velocity, p is the plasma pressure, $\mathbf{J}$ is the current density, $\mathbf{E}_0$ is the (uniform) externally driven inductive electric field, $\mathbf{F}_0$ is the externally applied force density, and $\Gamma = 5/3$ is the ratio of specific heats.

Let $(x/a, y/a, z/a) \rightarrow (x,y,z)$, $t/(a/V_A) \rightarrow t$, $\mathbf{B}/B_0 \rightarrow \mathbf{B}$, $\mathbf{A}/(B_0 a) \rightarrow \mathbf{A}$, $\mathbf{V}/V_A \rightarrow \mathbf{V}$, $\varphi/(B_0 V_A a) \rightarrow \varphi$, $p/(\rho V_A^2) \rightarrow p$, $\mathbf{J}/(B_0/\mu_0 a) \rightarrow \mathbf{J}$, $\mathbf{E}_0/(B_0 V_A) \rightarrow \mathbf{E}_0$, $\mathbf{F}_0/(\rho V_A^2/a) \rightarrow \mathbf{F}_0$, $\eta/\eta(0) \rightarrow \hat{\eta}$, $\eta(0)/(V_A a \mu_0) \rightarrow \eta$, and $\mu/(V_A a \rho) \rightarrow \mu$, where $V_A = B_0/\sqrt{\mu_0 \rho}$ is the Alfvén velocity, a a convenient scale-length, and B_0 a convenient scale magnetic field-strength.

[a)]Paper GI1 3, Bull. Am. Phys. Soc. **47**, 135 (2002).
[b)]Invited speaker. Electronic mail: rfitzp@farside.ph.utexas.edu

Let $\mathbf{A}(x,y)=[0,0,\psi(x,y)]$, $\mathbf{V}(x,y)=[u(x,y),v(x,y),0]$, $\mathbf{J}(x,y)=[0,0,J(x,y)]$, $\mathbf{E}_0(x,y)=[0,0,E_0]$, and $\mathbf{F}_0(x,y)=[0,F_0(x),0]$. It follows that

$$\frac{\partial u}{\partial t}=-u\frac{\partial u}{\partial x}-v\frac{\partial u}{\partial y}-\frac{\partial p}{\partial x}-\nabla^2\psi\frac{\partial \psi}{\partial x}+\mu\nabla^2 u, \tag{6}$$

$$\frac{\partial v}{\partial t}=-u\frac{\partial v}{\partial x}-v\frac{\partial v}{\partial y}-\frac{\partial p}{\partial y}-\nabla^2\psi\frac{\partial \psi}{\partial y}+\mu\nabla^2 v+F_0, \tag{7}$$

$$\frac{\partial \psi}{\partial t}=-u\frac{\partial \psi}{\partial x}-v\frac{\partial \psi}{\partial y}+\eta\hat{\eta}\nabla^2\psi+E_0, \tag{8}$$

$$\frac{\partial p}{\partial t}=-u\frac{\partial p}{\partial x}-v\frac{\partial p}{\partial y}-\Gamma p\left(\frac{\partial u}{\partial x}+\frac{\partial v}{\partial y}\right), \tag{9}$$

where $\nabla^2\equiv\partial^2/\partial x^2+\partial^2/\partial y^2$.

B. Plasma equilibrium

Suppose that the plasma is bounded by perfectly conducting walls located at $x=\pm X_w$, and is periodic in the y-direction with periodicity length L. The initial Harris-pinch plasma equilibrium satisfies

$$u^{(0)}(x)=0, \tag{10}$$

$$v^{(0)}(x)=V_0\cos\left(\frac{\pi}{2}\frac{x}{X_w}\right), \tag{11}$$

$$\psi^{(0)}(x)=-\ln\left(\frac{\cosh x}{\cosh X_w}\right)+\frac{x^2-X_w^2}{2\cosh^2 X_w}, \tag{12}$$

$$p^{(0)}(x)=\frac{1}{2}\left(\left[\tanh X_w-\frac{X_w}{\cosh^2 X_w}\right]^2-\left[\tanh x-\frac{x}{\cosh^2 X_w}\right]^2\right), \tag{13}$$

$$\hat{\eta}(x)=\cosh^2 x\left(\frac{\cosh^2 X_w-1}{\cosh^2 X_w-\cosh^2 x}\right). \tag{14}$$

Here, V_0 is the (normalized) unperturbed equilibrium flow speed at the magnetic resonance, $B_y^{(0)}=0$ (i.e., at $x=0$). Moreover, in unnormalized units, B_0 is the equilibrium field-strength as $x\to\infty$, and a is the half-width of the current channel. Note that $E_0=-\eta\hat{\eta}d^2\psi^{(0)}/dx^2$ and $F_0(x)=-\mu d^2v^{(0)}/dx^2$.

In the simple equilibrium described above there is no z-directed magnetic field and zero pressure gradient (in the x-direction) at the resonant surface (hence, pressure gradient effects play no role in the mode dynamics).

C. Boundary conditions

Suppose that the conducting wall at $x=X_w$ is subject to a *small* displacement $\Xi(y,t)$ in the x-direction. An equal and opposite displacement is applied to the wall at $x=-X_w$. Of course, the displacements are periodic in y, so that $\Xi(L,t)=\Xi(0,t)$. The appropriately modified *no-slip* boundary conditions at the walls are

$$u(X_w,y)=-u(-X_w,y)=\frac{\partial \Xi}{\partial t}, \tag{15}$$

$$v(X_w,y)=v(-X_w,y)=-\left[\frac{dv^{(0)}}{dx}\right]_{x=X_w}\Xi, \tag{16}$$

$$\psi(X_w,y)=\psi(-X_w,y)=-\left[\frac{d\psi^{(0)}}{dx}\right]_{x=X_w}\Xi, \tag{17}$$

$$p(X_w,y)=p(-X_w,y)=-\left[\frac{dp^{(0)}}{dx}\right]_{x=X_w}\Xi. \tag{18}$$

Furthermore, all fields satisfy $A(x,L)=A(x,0)$.

III. ERROR-FIELD PENETRATION THEORY

A. Asymptotic matching

Consider the response of a tearing-stable plasma to a wall displacement of the form $\Xi(y,t)=\xi(t)e^{iky}$, where $k=2\pi/L$. Here, it is assumed that the displacement amplitude, ξ, varies on a time scale which is *much longer* than any plasma time scale (just like error-fields in tokamaks).

Conventional theory divides the plasma into an *outer* and an *inner* region, with the latter region strongly localized in the vicinity of the magnetic resonance (i.e., $x=0$). In the outer region, plasma inertia, resistivity, viscosity, and compressibility can all be neglected. In this limit, Eqs. (6)–(9) reduce to the following equation:

$$\frac{d^2\psi^{(1)}}{dx^2}-k^2\psi^{(1)}-\frac{d^3\psi^{(0)}/dx^3}{d\psi^{(0)}/dx}\psi^{(1)}=0, \tag{19}$$

where the perturbed magnetic flux is written $\delta\psi(x,y)=\psi^{(1)}(x)e^{iky}$. In deriving the above equation, it is assumed that the wall perturbation is relatively low amplitude (which justifies a linear approach), and that the plasma flow speed is small compared to both the sound and Alfvén speeds. The boundary conditions at the conducting walls are written

$$\psi^{(1)}(\pm X_w)=-\frac{d\psi^{(0)}(X_w)}{dx}\xi. \tag{20}$$

Moreover, from symmetry, $\psi^{(1)}(-x)=\psi^{(1)}(x)$. Hence, asymptotic matching to the inner region yields

$$\Psi=\frac{E_{sw}\xi}{\Delta-E_{ss}}, \tag{21}$$

where E_{ss} and E_{sw} are real numbers obtained by solving Eq. (19) subject to the boundary conditions and symmetry constraints. The complex quantity $\Psi=\lim_{x\to 0}\psi^{(1)}(x)$ is the reconnected magnetic flux (assuming a constant-ψ inner regime) driven by the wall perturbation. The complex quantity Δ parameterizes the response of the inner region to the wall perturbation. Note that E_{ss} is the conventional tearing stability index (for the wavelength L tearing mode).[7] The plasma is intrinsically stable (to the wavelength L tearing mode) provided that $E_{ss}<0$.

B. Layer physics

The main premise of the analytic theory developed in Refs. 4–6 is that the inner response of a flowing plasma to a static external magnetic perturbation, for the case in which driven reconnection is strongly flow suppressed, is well described by *linear*, *constant-ψ* layer physics. Now, the response regime which is most appropriate to ohmically heated tokamak plasmas is the so-called *viscoresistive regime*,[6] in which plasma inertia and compressibility play a negligible role. The response of a viscoresistive layer to an external perturbation is described by the following expression:[8]

$$\Delta = i\mathcal{A}\frac{k^{2/3}}{s^{1/3}} V \mu^{1/6} \eta^{-5/6}. \tag{22}$$

Here, V is the y-component of the equilibrium flow velocity at the magnetic resonance (i.e., $x=0$), whereas $s = |d^2\psi^{(0)}/dx^2|_{x=0}$, and $\mathcal{A} = 6^{2/3}\pi\Gamma(5/6)/\Gamma(1/6) = 2.104$.

The viscoresistive regime holes in the high viscosity limit, $\mu \gg \eta$, provided[8]

$$V \ll \frac{\eta^{2/3}}{\mu^{1/3}}. \tag{23}$$

Likewise, the viscoresistive regime holds in the low viscosity limit, $\mu \ll \eta$, provided[8]

$$V \ll \frac{\mu^{2/3}}{\eta^{1/3}}. \tag{24}$$

The neglect of plasma compressibility in the layer is justified as long as V remains well below the velocity of sound.

C. Force balance

The net y-directed electromagnetic force exerted on the inner region (zero net force is exerted on the outer region) by the wall perturbation is written[4–6]

$$F_{yEM} = -\frac{k}{2}|\Psi|^2\ \mathrm{Im}(\Delta). \tag{25}$$

The net y-directed viscous restoring force acting on the inner region takes the form,[4–6]

$$F_{yVS} = \frac{2\mu}{X_w}(V_0 - V). \tag{26}$$

In deriving the above expression, it is assumed that the plasma is in a *quasi-steady-state* (since the wall perturbation varies very slowly in time). Of course, in a *quasi-steady-state* the total y-directed force acting on the inner region must be zero, i.e., $F_{yEM} + F_{yVS} = 0$. Note that the $(\mathbf{V}\cdot\nabla)\mathbf{V}$ force is assumed to be negligible compared to the electromagnetic and viscous forces.

Equations (21), (22), (25), and (26) (plus the force balance requirement) yield

$$4\left(1 - \frac{V}{V_0}\right)\frac{V}{V_0} = \frac{(V/V_0)^2}{(V/V_0)^2 + \alpha^2}\left(\frac{|\xi|}{\xi_c}\right)^2, \tag{27}$$

where

$$\xi_c = \frac{\sqrt{\mathcal{A}}}{(sk)^{1/6} E_{sw}\sqrt{X_w}} V_0 \mu^{7/12}\eta^{-5/12}, \tag{28}$$

and

$$\frac{1}{\alpha} = \frac{\mathcal{A}}{|E_{ss}|}\frac{k^{2/3}}{s^{1/3}} V_0 \mu^{1/6}\eta^{-5/6}. \tag{29}$$

Furthermore, Eq. (21) gives

$$\frac{|\Psi|}{\Psi_{\mathrm{full}}} = \frac{\alpha}{\sqrt{(V/V_0)^2 + \alpha^2}}, \tag{30}$$

where $\Psi_{\mathrm{full}} = E_{sw}|\xi|/|E_{ss}|$ is the driven reconnected flux in the absence of a plasma flow.

According to Eqs. (27) and (30), when the parameter α is much less than unity (which is always the case in tokamak plasmas), externally driven reconnection is strongly flow suppressed (i.e., $|\Psi| \ll \Psi_{\mathrm{full}}$) provided the perturbation amplitude, $|\xi|$, remains below the critical value, ξ_c. In fact, in this situation,

$$\frac{V}{V_0} \simeq \frac{1 + \sqrt{1 - (|\xi|/\xi_c)^2}}{2}, \tag{31}$$

$$\frac{|\Psi|}{\Psi_{\mathrm{full}}} \simeq \frac{2\alpha}{1 + \sqrt{1 - (|\xi|/\xi_c)^2}}. \tag{32}$$

However, as soon as the perturbation amplitude rises above the critical value, the flow suppressed state ceases to exist, and the system make a transition to a state in which the plasma flow at the magnetic resonance is arrested (i.e., $V \rightarrow 0$), and driven reconnection proceeds unhindered (i.e., $|\Psi| \rightarrow \Psi_{\mathrm{full}}$). Note that the perturbation amplitude must be reduced well below the critical amplitude before the reverse transition is triggered. (See Ref. 6 for more details regarding these transitions.)

Expression (28) (which is easily generalized to cylindrical geometry) is widely used to estimate the maximum tolerable error-field amplitude in tokamaks (if error-field driven reconnection problems are to be avoided). The aim of this paper is to benchmark Eq. (28) against the results of nonlinear MHD simulations.

IV. NUMERICAL RESULTS

A. Introduction

Equations (6)–(9), plus the initial equilibrium (10)–(14) and the boundary conditions (15)–(18), have been implemented numerically in a finite-difference code which is second-order in space and first-order in time. The code makes use of the well-known semi-implicit algorithm of Harned and Schnack[9] in order to circumvent the highly restrictive Courant–Freidrichs–Lewy condition on the Alfvén wave. The computational grid is uniform in the y-direction. However, in the x-direction the grid points are more closely packed in the vicinity of the magnetic resonance, in order to help resolve the reconnecting layer. All the simulations discussed in this paper employ a uniform time step of 0.5 normalized time units, as well as a 128×64 computational grid.

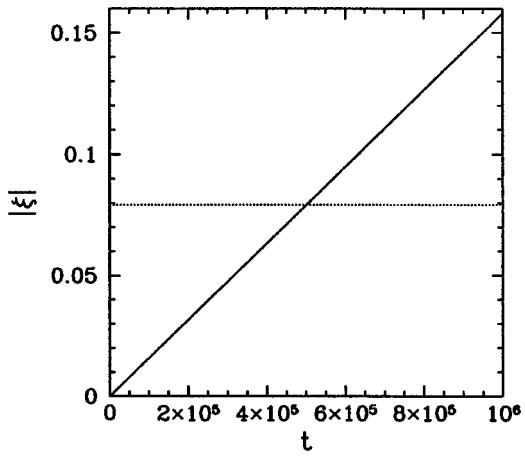

FIG. 1. The amplitude, $|\xi|$, of the wall displacement vs time for a nonlinear simulation performed with $X_w=2.5$, $L=5$, $V_0=1\times10^{-2}$, $\mu=1\times10^{-2}$, and $\eta=1\times10^{-4}$. The horizontal dotted line indicates the value of ξ_c.

B. Example calculation

Figures 1–3 show data obtained from a nonlinear simulation performed with the following plasma parameters: $X_w=2.5$, $L=5$, $V_0=1\times10^{-2}$, $\mu=1\times10^{-2}$, and $\eta=1\times10^{-4}$. For these parameters, it can be demonstrated that $k=1.257$, $s=0.9734$, $E_{ss}=-0.8939$, $E_{sw}=0.3539$, $\alpha=3.616\times10^{-2}$, and $\xi_c=7.928\times10^{-2}$.

As can be seen from Fig. 1, the amplitude of the wall perturbation is ramped *linearly* from zero over 10^6 normalized time-units (as is the case in all of the simulations discussed in this paper). This variation time scale is much longer than any plasma time scale; hence, it is reasonable to suppose that the plasma remains in a quasi-steady-state in the presence of the perturbation, as was assumed in the previous theoretical discussion.

Figures 2 and 3 demonstrate that when the perturbation amplitude lies well below the critical value (i.e., $|\xi|\ll\xi_c$), the plasma flow is unaffected (i.e., $V=V_0$), and the reconnected flux takes the strongly flow suppressed value $\alpha\Psi_{\rm full}$. As $|\xi|$ approaches ξ_c, the equilibrium flow velocity at the magnetic resonance gradually slows down, and there is a simultaneous gradual rise in the reconnected flux. However, as soon as the critical perturbation amplitude is exceeded, there is a sudden collapse in the plasma flow at the magnetic resonance, accompanied by a very substantial, and equally sudden, rise in the reconnected flux. The behavior shown in Figs. 1–3 is in very good agreement with the theory outlined in Sec. III (note, in particular, that the theory accurately predicts the values of ξ_c and the flow suppressed reconnected flux), and is also similar to that observed experimentally.[2]

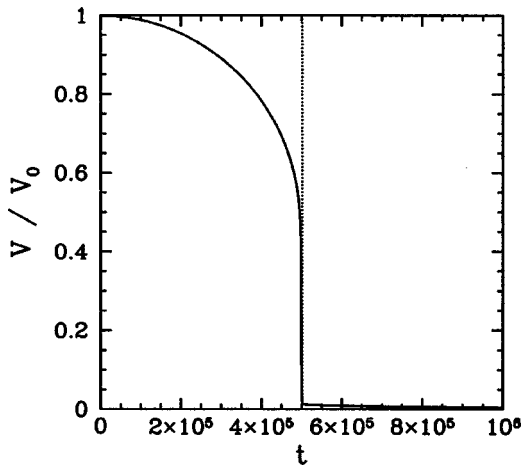

FIG. 2. The net y-directed plasma flow velocity, V, at the magnetic resonance (normalized with respect to its unperturbed value, V_0) vs time for a nonlinear simulation performed with $X_w=2.5$, $L=5$, $V_0=1\times10^{-2}$, $\mu=1\times10^{-2}$, and $\eta=1\times10^{-4}$. The vertical dotted line indicates the time at which $|\xi|=\xi_c$.

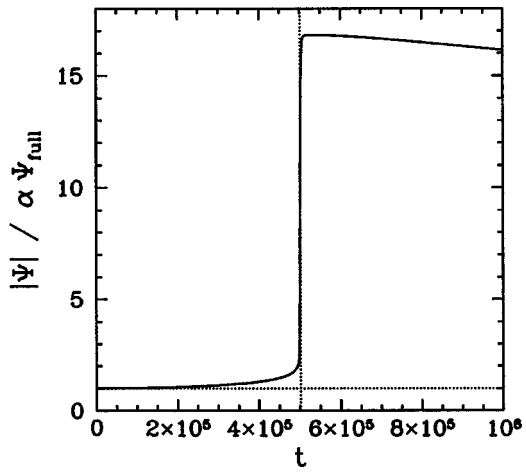

FIG. 3. The magnitude of the reconnected magnetic flux, $|\Psi|$, (normalized with respect to the expected flux, $\alpha\Psi_{\rm full}$, in the fully flow suppressed case) vs time for a nonlinear simulation performed with $X_w=2.5$, $L=5$, $V_0=1\times10^{-2}$, $\mu=1\times10^{-2}$, and $\eta=1\times10^{-4}$. The vertical dotted line indicates the time at which $|\xi|=\xi_c$.

C. Scans of major plasma parameters

The scans of major plasma parameters reported in this paper are performed at constant (theoretical) ξ_c and α. This is possible as long as $\eta\propto V_0$ and $\mu\propto1/V_0$. Figure 4 shows the scan trajectories through $\mu-\eta$ space. Note that a very wide range of μ and η values is covered. It is helpful to define $P=\mu/\eta$ and $Q=V_0/\eta^{1/3}$. The viscoresistive regime extends over the domains $Q\ll P^{-1/3}$ for $P\gg1$, and $Q\ll P^{1/3}$ for $P\ll1$ (see Sec. III). Figure 5 shows the scan trajectories through $Q-P$ space, indicating the boundaries of the viscoresistive regime. It can be seen that the scans make a fairly thorough exploration of the experimentally relevant high-flow limit of the viscoresistive regime. The parameter scans are performed with the following auxiliary plasma parameters: $X_w=2.5$ and $L=5$.

Figure 6 shows the numerically determined critical perturbation amplitude, ξ_c (actually, the perturbation amplitude at which $V=0.1V_0$) vs the unperturbed plasma flow speed, V_0, for the various scans described above. Also shown are the theoretical ξ_c values. It can be seen that, although V_0 is varied by about three orders of magnitude during each scan, the numerically determined ξ_c value remains approximately constant, in accordance with theory [i.e., since expression (28) is invariant with V_0 if $\eta\propto V_0$ and $\mu\propto1/V_0$]. Moreover,

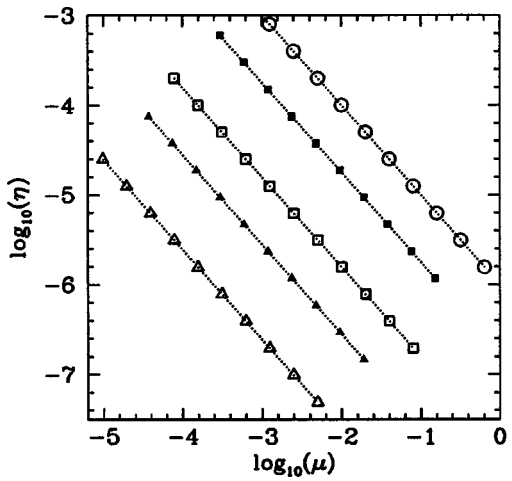

FIG. 4. Scan trajectories through $\mu-\eta$ space. The open triangular points correspond to $\mu=9.766\times10^{-8}/V_0$ and $\eta=2.500\times10^{-3}V_0$. The solid triangular points correspond to $\mu=7.418\times10^{-7}/V_0$ and $\eta=3.750\times10^{-3}V_0$. The open square points correspond to $\mu=3.125\times10^{-6}/V_0$ and $\eta=5.000\times10^{-3}V_0$. The solid square points correspond to $\mu=2.373\times10^{-5}/V_0$ and $\eta=7.500\times10^{-3}/V_0$. The open round points correspond to $\mu=1.000\times10^{-4}/V_0$ and $\eta=1.000\times10^{-2}V_0$. The auxiliary plasma parameters are $X_w=2.5$ and $L=5$.

the numerical determined ξ_c values are in extremely good agreement with the corresponding theoretical values. Hence, the data presented in Fig. 6 effectively validate the V_0, μ, and η scalings of the error-field penetration formula, (28).

Note, from Fig. 6, that there is a small deviation between the numerically determined and theoretical critical perturbation amplitudes at large V_0. As can be seen from Fig. 5, this deviation occurs because at large V_0 the various scans approach the lower boundary of the viscoresistive regime in $Q-P$ space. Of course, the theoretical formula (28) is only valid well within the viscoresistive regime. Any deviation between the numerical and theoretical critical perturbation amplitudes at low V_0 is caused by the reconnection time scale increasing to such an extent that the plasma response to the external perturbation is no longer quasi-steady-state. Finally, the deviation between the numerical and theoretical critical perturbation amplitudes evident in the low ξ_c scans in Fig. 6 (which are also low η and μ scans) is due to spatial resolution problems caused by the narrowness of the reconnecting layer.

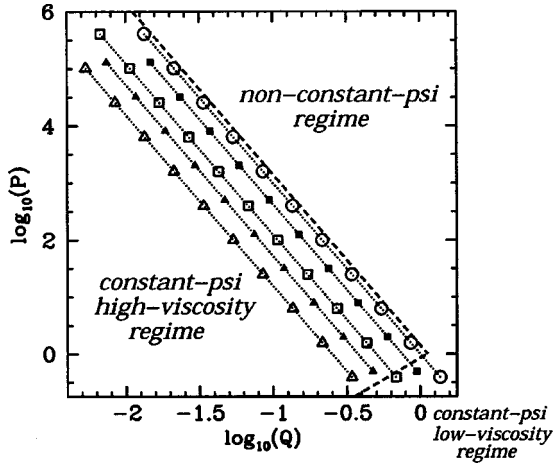

FIG. 5. Scan trajectories through $Q-P$ space. The dashed lines indicate the right and lower boundaries of the viscoresistive regime. The key for the different scans is the same as in Fig. 4. The auxiliary plasma parameters are $X_w=2.5$ and $L=5$.

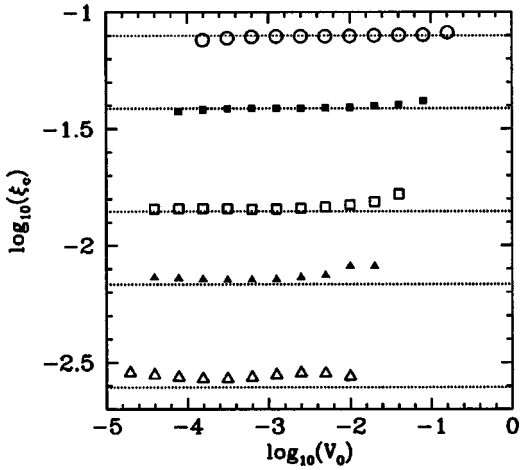

FIG. 6. The numerically determined critical perturbation amplitude, ξ_c, vs the unperturbed plasma flow speed, V_0. The dotted horizontal lines indicate the corresponding theoretical ξ_c values. The key for the different scans is the same as in Fig. 4. The auxiliary plasma parameters are $X_w=2.5$ and $L=5$.

D. Scans of auxiliary plasma parameters

The dependence of the error-field penetration formula, (28), on the auxiliary plasma parameters X_w and L is rendered nontrivial by the presence of the E_{sw} factor. The value of E_{sw} is obtained by solving Eq. (19), subject to the boundary condition (20), and possesses no simple analytic dependence on X_w and L.

Figure 7 details the dependence of the numerically de-

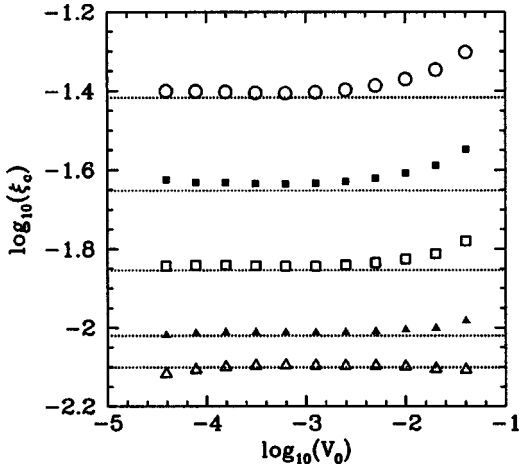

FIG. 7. The numerically determined critical perturbation amplitude, ξ_c, vs the unperturbed plasma flow speed, V_0. The dotted horizontal lines indicate the corresponding theoretical ξ_c values. All scans are performed with $\mu=3.125\times10^{-6}/V_0$, $\eta=5.000\times10^{-3}V_0$, and $L=5$. The open triangular points correspond to $X_w=1.5$. The solid triangular points correspond to $X_w=2.0$. The open square points correspond to $X_w=2.5$. The solid square points correspond to $X_w=3.0$. The open circular points correspond to $X_w=3.5$.

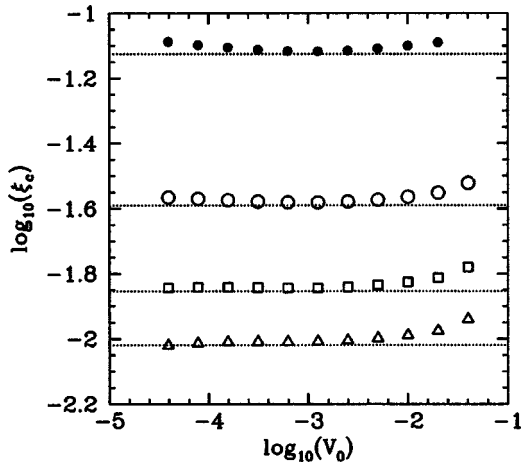

FIG. 8. The numerically determined critical perturbation amplitude, ξ_c, vs the unperturbed plasma flow speed, V_0. The dotted horizontal lines indicate the corresponding theoretical ξ_c values. All scans are performed with $\mu = 3.125\times 10^{-6}/V_0$, $\eta = 5.000\times 10^{-3}V_0$, and $X_w = 2.5$. The open triangular points correspond to $L = 6.0$. The open square points correspond to $L = 5.0$. The open round points correspond to $L = 4.0$. The solid round points correspond to $L = 3.0$.

termined critical perturbation amplitude, ξ_c, on the conducting wall position, X_w. Also shown are the theoretical ξ_c values. It can be seen that there is excellent agreement between the numerical and theoretical ξ_c values.

Figure 8 details the dependence of the numerically determined critical perturbation amplitude, ξ_c, on the plasma periodicity length, L. Also shown are the theoretical ξ_c values. Again, it can be seen that there is excellent agreement between the numerical and theoretical ξ_c values.

The data presented in Figs. 7 and 8 effectively validate the X_w and L scalings of the error-field penetration formula, (28).

V. SUMMARY AND CONCLUSIONS

The error-field penetration formula, (28), has been successfully benchmarked against nonlinear MHD simulations in slab geometry. Furthermore, the fundamental assumption underlying the derivation of Eq. (28)—namely, that the response of a flowing plasma to a low amplitude, quasistatic, resonant magnetic perturbation is governed by *linear*, *constant-ψ* layer physics—has been verified over a wide range of plasma parameters, which includes the parameter range relevant to ohmic and neutral beam injection (NBI) start-up discharges in modern-day tokamaks. Hence, formula (28) can be used to estimate error-field penetration thresholds in such plasmas.

Error-field penetration was first investigated numerically by Parker.[11,12] The results reported in Refs. 11 and 12 are broadly consistent (but far less conclusive) with those described here.

Equation (28) is easily generalized to cylindrical geometry.[4–6] In large aspect-ratio toroidal geometry, poloidal flow damping effects cause the plasma to only response to the relatively small toroidal component of the error-field locking torque. This effect (which is perfectly calculable) gives rise to a substantial increase in the critical error-field amplitude required to trigger driven magnetic reconnection.[4–6] Toroidal coupling effects (which are also calculable) can also significantly modify the critical error-field amplitude, especially in highly shaped discharges.[10]

In plasmas which are rapidly rotating, due to unbalanced NBI, the constant-ψ approximation breaks down in the reconnecting layer[6] [the criterion for the breakdown of the constant-ψ approximation is given in Eq. (23)]. Hence, the response of such plasmas to quasi-static, resonant magnetic perturbation is not governed by Eq. (28). Large tokamaks subject to intense auxiliary heating tend to become effectively collisionless. It follows that the collisional formula, (28), does not apply to such plasmas either. Error-field penetration in both strongly rotating and collisionless plasmas will be the subject of future investigations.

ACKNOWLEDGMENTS

This research was funded by the U.S. Department of Energy under Contract No. DE-FG05-96ER-54346 as well as via Cooperative Agreement No. DE-FC02-01ER54652 under the auspices of the program for Scientific Discovery through Advanced Computing.

[1] J. T. Scoville, R. J. La Haye, A. G. Kellman, T. H. Osborne, R. D. Stambaugh, E. J. Strait, and T. S. Taylor, Nucl. Fusion **31**, 875 (1991).
[2] T. C. Hender, R. Fitzpatrick, A. W. Morris, P. G. Carolan, R. D. Durst, T. Edlington, J. Ferreira, S. J. Fielding, P. S. Haynes, J. Hugill, I. J. Jenkins, R. J. La Haye, B. J. Parham, D. C. Robinson, T. N. Todd, M. Valovič, and G. Vayakis, Nucl. Fusion **32**, 2091 (1992).
[3] G. M. Fishpool and P. S. Haynes, Nucl. Fusion **34**, 109 (1994).
[4] R. Fitzpatrick, in *Theory of Fusion Plasmas, Proceedings of the Joint Varenna-Lausanne International Workshop*, Varenna, 1992 (Società Italiana di Fisica, Bologna, 1992), p. 147.
[5] R. Fitzpatrick, Nucl. Fusion **33**, 1049 (1993).
[6] R. Fitzpatrick, Phys. Plasmas **5**, 3325 (1998).
[7] H. P. Furth, J. Killeen, and M. N. Rosenbluth, Phys. Fluids **6**, 459 (1963).
[8] R. Fitzpatrick, Phys. Plasmas **1**, 3308 (1994).
[9] D. S. Harned and D. D. Schnack, J. Comput. Phys. **65**, 57 (1986).
[10] R. Fitzpatrick and T. C. Hender, Phys. Plasmas **1**, 3337 (1994).
[11] R. D. Parker, in *Theory of Fusion Plasmas, Proceedings of the Joint Varenna-Lausanne International Workshop*, Varenna, 1992 (Editrice Compositiori, Bologna, 1992), p. 399.
[12] R. D. Parker, in *Proceedings of the 1992 International Conference on Plasma Physics*, Innsbruck, 1992 (European Physical Society, Petit-Lancy, 1992), Vol. 1, p. 427.